IEEE Access
Multidisciplinary ⋮ Rapid Review ⋮ Open Access Journal

Received 8 March 2023, accepted 29 March 2023, date of publication 10 April 2023, date of current version 13 April 2023.

*Digital Object Identifier 10.1109/ACCESS.2023.3265957*

RESEARCH ARTICLE

# A Novel Neural Network-Based Robust Adaptive Formation Control for Cooperative Transport of a Payload Using Two Underactuated Quadcopters

**LUIS F. CANAZA CCARI[1] AND PABLO RAUL YANYACHI[1,2], (Senior Member, IEEE)**
[1]Department of Electronic Engineering, Universidad Nacional de San Agustín de Arequipa, Arequipa 04000, Peru
[2]Instituto de Investigación Astronómico y Aeroespacial Pedro Paulet, Universidad Nacional de San Agustín de Arequipa, Arequipa 04000, Peru
Corresponding author: Luis F. Canaza Ccari (lcanazacc@unsa.edu.pe)

**ABSTRACT** Designing a controller for the cooperative transport of a payload using quadcopter-type unmanned aerial vehicles (UAVs) is a very challenging task in control theory because these vehicles are underactuated mechanical systems. This paper presents a novel robust adaptive formation control design for the cooperative transport of a suspended payload by ropes using two underactuated quadcopters in the presence of external disturbances and parametric uncertainties. The structure of the proposed controller is divided into two subsystems: fully actuated and underactuated. An integral sliding mode adaptive control strategy is proposed for the fully actuated subsystem, and for the underactuated subsystem, an adaptive control strategy based on the combination of Backstepping and sliding mode is proposed. Then, the control parameters of the sliding surfaces of both control subsystems are adaptively tuned by a neural network. In addition, to improve the robustness of the proposed controller, a disturbance observer is incorporated to estimate and compensate for the lumped disturbances. The asymptotic stability of the cooperative transport system is verified with the Lyapunov theorem. Finally, numerical simulations are performed in MATLAB/Simulink environment, and the results show that the proposed controller successfully transports the payload safely and without oscillations. Moreover, the desired formation pattern is maintained throughout the flight task, even with external disturbances and parametric uncertainties.

**INDEX TERMS** Robust adaptive control, cooperative payload transportation, quadcopters, underactuated, UAVs.

## I. INTRODUCTION

### A. CONTEXT AND MOTIVATIONS

Quadcopters are very versatile unmanned aerial vehicles (UAV) due to their diverse capabilities for civilian and military applications [1]. Cooperative payload transport is one of the applications that has recently attracted the attention of researchers [2] because it can be used for transporting medical packages to rural areas that are difficult to access [3], transporting tanks with chemicals for crop spraying [4], transporting loads for construction processes [5], etc.

A quadcopter is an underactuated mechanical system with six degrees of freedom and four control inputs, i.e., the control action cannot act independently in all degrees of freedom [6], [7]. Now, when a quadcopter is attached to a suspended payload, the underactuated mechanical system is more difficult to control due to unknown nonlinear characteristics, dynamic coupling, and payload oscillations. In this context, research has been conducted on payload transport with a single quadcopter [8], [9], [10]; these works mainly aim to stabilize the quadcopter and reduce payload oscillations. However, transporting a payload with a single quadcopter presents some limitations, such as payload weight, payload oscillations, and intolerance to failure [11]. The solution to this problem is using several quadcopters to carry a payload using a multi-agent system widely used in the literature for multi-quadcopter flight formation [12], [13], [14]. Using multi-quadcopters for transport improves

The associate editor coordinating the review of this manuscript and approving it for publication was Min Wang.

payload performance, i.e., heavier payloads can be transported, greater control of oscillations, and the ability to complete the transport task even if one quadcopter fails. However, designing a control strategy for the flight formation of multiple quadcopters carrying a payload is even more complicated. Such complications are due to the communication between the quadcopters and the suspended payload for flight formation, coupled nonlinear dynamics, and that quadcopters are underactuated mechanical systems, the latter being a crucial property for control design and has not been considered as such in many research works. Therefore, the control design for a quadcopter as an underactuated mechanical system requires a nonlinear control strategy suitable and reliable for the cooperative transport of a payload.

This paper investigates the control design for the cooperative transport of a payload using two underactuated quadcopters. Therefore, the main objective of the paper is to transport the payload safely and with minimal oscillation while maintaining the desired formation pattern and stability of the underactuated quadcopters with the payload suspended.

### B. LITERATURE REVIEW ON THE COOPERATIVE TRANSPORT OF A PAYLOAD USING QUADCOPTERS

There are several research works on cooperative payload transport using quadcopters, such as payload transport by gripping with a robotic arm [15], [16], [17] and payload transport using cables or ropes [18], [19], [20], [21], [22]. Each of these methods has its advantages and disadvantages; in the use of gripping with a robotic arm, the payload does not oscillate, but it causes increased inertia, high cost, and high energy consumption. On the other hand, the use of cables or ropes is more popular due to its simplicity and low cost, but it causes an increase in the degrees of freedom in quadcopters due to payload oscillations which leads to a more complicated control design.

In this context, several efforts have been made to address the control design for the cooperative transport of a suspended payload using ropes. For example, some linear control techniques such as Proportional, Integral and Derivative (PID) [23], [24], [25], [26] and Linear Quadratic Regulator (LQR) [27], [28] have been used. In research [23] using two UAVs for cooperative transportation, an adaptive kinematic PID controller based on null space theory is proposed. In [24], a trajectory planning method is proposed using three quadcopters for cooperative transport, and a dual cascade PID control is designed for trajectory tracking. In [25], using four quadcopters for cooperative transport, a PID controller is proposed for quadcopter motion and PD for load swing control. In [26], an LQR-PID control strategy is designed for cooperative transport using four quadcopters and proposes a guidance algorithm using a virtual leader scheme based on payload position. In [27], a leader-follower scheme is implemented using two quadcopters; the authors propose a hierarchical control; for the position, an LQR control is implemented, and for the attitude, a Quaternion-based controller is implemented. In [28], two quadcopters are also used for cooperative transport, and an iterative LQR control is proposed. Some nonlinear control techniques have also been used to address the cooperative transport of a payload using quadcopters. Research works [29], [30], [31] proposes a nonlinear control strategy based on feedback linearization for cooperative transport; however, such a control strategy is not useful for the control of underactuated mechanical systems because it cannot cancel the undesirable dynamics of underactuated quadcopters [6]. In [32], a predictive control strategy for transporting a payload employing four quadcopters is proposed. In [33], Backstepping control is proposed for cooperative transport under suspension failures, and a disturbance observer is designed to estimate the rope tension forces.

In the previous research, different linear and nonlinear control strategies were designed to address for the cooperative transport of a payload. However, the authors did not consider the underactuated property of quadcopters for the control design, i.e., they designed one control action for each degree of freedom, which is not fulfilled in underactuated mechanical systems such as quadcopters that have four inputs and six outputs. In contrast, in our paper, we consider the underactuated property of quadcopters for control design, which is the main novelty of the paper, i.e., for each underactuated quadcopter, only four control inputs are designed to perform the cooperative transport task.

### C. STATE OF THE ART OF RELATED WORK

In the literature, there are research works that did focus on the control design for a quadcopter as an underactuated mechanical system, i.e., four control inputs were designed for six degrees of freedom; these studies were based on sliding mode [34], [35], [36], [37], [38] and Backstepping [39], [40] control techniques. However, only trajectory tracking control was addressed, but not formation control for a cooperative transport system, although it is worth noting that research works [37], [38] used neural networks to estimate unknown nonlinearities and external disturbances, improving the robustness of the controller. In this sense, using neural networks for control design provides an adaptive method to handle unknown external disturbances, which are good candidates for a cooperative payload transport application.

To the best of our knowledge, a robust adaptive formation control for the cooperative transport of a payload using quadcopters as underactuated mechanical systems has not been designed in the literature. Although, recently in [41], [42], control design for payload transport with a single quadcopter as an underactuated mechanical system was addressed, where in [41] proposes a sliding neuro-mode controller, and in [42] proposes a finite-time sliding neuro-mode controller. However, they did not address formation control for cooperative transport; moreover, in their results, they only present the

temporal response of the quadcopter but not the temporal response of the suspended payload, thus the effectiveness of the proposed controller to suppress oscillations of a suspended payload, which is one of the main limitations of suspended payload transport with a single quadcopter, cannot be guaranteed. In contrast, our work does present the temporal response of the quadcopters and the suspended payload when cooperative transport is performed.

When addressing the cooperative transport of a payload, the rope tension forces generated by the weight of the payload will significantly impact the dynamics and stability of the quadcopters because these tension forces cannot be measured directly. An efficient solution is to incorporate a disturbance observer into the controller to compensate for all types of disturbances, both external and internal. In [18] and [33], the authors consider the rope tensions as an external disturbance and estimate it with a disturbance observer. However, these works do not consider disturbances like wind gusts and parametric uncertainties.

### D. CONTRIBUTIONS

Motivated by the previous research works, this paper presents a novel control design for the cooperative transport of a payload using two quadcopters which are considered an underactuated mechanical system. The main contributions of the present paper are as follows:

- A novel robust adaptive formation controller is designed for the cooperative transport of a payload suspended by ropes using two underactuated quadcopters. For this purpose, the controller structure is divided into two subsystems: fully actuated and underactuated. An integral sliding mode adaptive control strategy is proposed for the fully actuated subsystem, and for the underactuated subsystem, an adaptive control strategy based on the combination of Backstepping and sliding mode is proposed. In addition, a neural network is used to adaptively tune the control parameters of the sliding surfaces in both control subsystems. To the best of our knowledge, this is the first time in the literature that control design for cooperative transport using quadcopters as underactuated mechanical systems is addressed.
- In this paper, external disturbances (unmeasurable rope tensions, wind gusts) and internal disturbances (parametric uncertainties) have been considered for the cooperative transport of a payload; all these disturbances constitute the total lumped disturbances and are estimated with a nonlinear disturbance observer.
- In comparison to [18] and [26], [33], where three and four quadcopters are used to transport a payload with the same weight. The proposed control strategy in this paper uses only two underactuated quadcopters to transport the same payload, demonstrating the higher robustness of the proposed controller against disturbances.

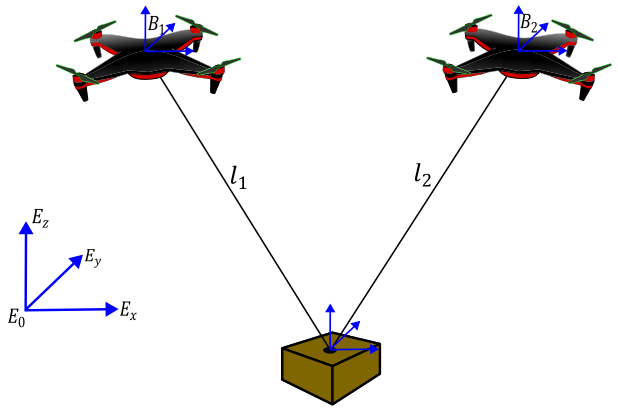


**FIGURE 1.** The cooperative transport system of a payload using two quadcopters.

### E. MANUSCRIPT ORGANIZATION

In II, the dynamic model is developed. In III, the flight formation of the cooperative transport system is presented. In IV, the four control inputs for each quadcopter are designed. The results of the numerical simulations are discussed in V. Finally, in VI, the conclusions of the paper are presented.

## II. DYNAMIC MODEL

In this section, the dynamic model of the underactuated quadcopters and the suspended payload is developed. Fig. 1 shows a representation of cooperative transport using two quadcopters, two ropes of length $l_1$ and $l_2$, and a suspended payload. Throughout the paper, the subscript $i$ corresponds to the $i$-th quadcopter ($i = 1, 2, \ldots n$).

### A. QUADCOPTER DYNAMIC MODEL

The $i$-th quadcopter as a rigid body is characterized by a body-fixed frame $B_i = \{x_B, y_B, z_B\}$ and an earth-fixed frame $E_0 = \{x_E, y_E, z_E\}$ (see Fig. 1). The vector $\xi_i = [x_i, y_i, z_i]^T$ and the vector $\eta_i = [\phi_i, \theta_i, \psi_i]^T$ describe the position and orientation of the $i$-th quadcopter in the $E$ frame, where $\phi$, $\theta$, and $\psi$ represent the Euler angles roll, pitch and yaw respectively. The rotation matrix $R_i : B_i \Rightarrow E$, is the transformation matrix from the body-fixed frame to the earth-fixed frame and is defined by:

$$R_i = \begin{bmatrix} c\psi c\theta & c\psi s\theta s\phi - s\psi c\phi & c\psi s\theta c\phi + s\psi s\phi \\ s\psi c\theta & s\psi s\theta s\phi + c\psi c\phi & s\psi s\theta c\phi - c\psi s\phi \\ -s\theta & c\theta s\phi & c\theta c\phi \end{bmatrix}. \tag{1}$$

where $c(\cdot) = cos(\cdot)$, $s(\cdot) = sin(\cdot)$. Using the Newton Euler mathematical approach, the translational and rotational dynamics of the $i$-th quadcopter are described by [20]:

$$\begin{cases} m_{qi}\ddot{\xi}_i = U_{1i}R_ie_z - m_{qi}ge_z - \mathbb{T}_i \times r_i + \delta_p(t), \\ J_i\ddot{\eta}_i = -\dot{\eta}_i \times J_i\dot{\eta}_i - \sum_{k=1}^{4} J_{ri}(\dot{\eta}_i \times e_z)(-1)^{k+1}\Omega_k \\ \qquad + U_i^{\tau} + \delta_{\Theta}(t). \end{cases} \tag{2}$$

Where $\xi_i = [x_i, y_i, z_i]^T \in \mathbb{R}^3$, $m_{qi} \in \mathbb{R}^+$, and $g \in \mathbb{R}^+$ represent the position, mass, and gravity acceleration of the $i$-th quadcopter. $U_{1i} \in \mathbb{R}^+$ is the magnitude of the total thrust generated by the four rotors, and $R_i \in \mathbb{R}^{3\times3}$ is the rotation matrix. $\mathbb{T}_i = [\mathbb{T}_x, \mathbb{T}_y, \mathbb{T}_z]^T \in \mathbb{R}^3$ represents the vector of the rope tension force acting on each quadcopter. Likewise, $\eta_i = [\phi_i, \theta_i, \psi_i]^T \in \mathbb{R}^3$, $J_i \in \mathbb{R}^{3\times3}$ represents the orientation and moment of inertia, and similarly, the moment and velocity of inertia of the rotors of the $i$-th quadcopter are denoted respectively by $J_{ri} \in \mathbb{R}^+$ and $\Omega_k \in \mathbb{R}^+$. The vector $U_i^\tau = [\varsigma U_{2i}, \varsigma U_{3i}, \kappa U_{4i}]^T \in \mathbb{R}^3$ represents the input torques, where $\varsigma$ represents the distance from the rotors to the center of the quadcopter, i.e., arm length, and $\kappa$ is the drag coefficient [43]. The matrix $\dot{\eta}_i\times = S(\dot{\eta}_i) \in \mathbb{R}^{3\times3}$ is a skew-symmetric matrix, where $\times$ denotes the vector cross product, $e_z = [0, 0, 1]^T \in \mathbb{R}^3$ is a unit vector, and finally, $\delta_p(t)$ and $\delta_\Theta(t)$ are external disturbances of the translation and rotation dynamics, respectively.

### B. PAYLOAD DYNAMIC MODEL

The payload is assumed to be on the ground initially. Therefore, the dynamics of payload is described by [20]:

$$\begin{cases} m_p\ddot{\xi}_p = -m_p g e_z + \sum_{i=1}^{n} \mathbb{T}_i \times r_i, \\ J_p\ddot{\eta}_p = -\dot{\eta}_p \times J_p\dot{\eta}_p - \sum_{k=1}^{n} \mathbb{T}_i \times r_i. \end{cases} \tag{3}$$

where $\xi_p \in \mathbb{R}^3$, $\eta_p \in \mathbb{R}^3$, $m_p \in \mathbb{R}^+$ and $J_p \in \mathbb{R}^+$ represent the position, orientation, mass, and moment of inertia of the payload, respectively. $\sum_{i=1}^{n} \mathbb{T}_i$ is the sum of the tension forces of the $n$ ropes acting on the payload, and finally, $r_i \in \mathbb{R}^3$ is a vector from the center of mass of the payload to the point of attachment of the ropes.

### C. THE UDWADIA-KALABA EQUATION

The tension forces of the ropes connected to the quadcopters are constraint forces and can be obtained using the Udwadia-Kalaba equations [26], [44]. This method provides explicit equations of the constraint forces, which are functions of the states of all the bodies involved and, therefore, are the most suitable for simulation purposes [45].

Consider the $i$-th rope connecting the $i$-th quadcopter with the payload. The constraint of the $i$-th rope can be defined as:

$$\varrho_i = \|\pounds_i\|^2 - {l_i}^2. \tag{4}$$

where $\pounds_i = \xi_i - \xi_p$, $l_i$ is the nominal length of the $i$-th rope. Differentiating two times (4), the cooperative transport system constraint can be formulated in its standard form as:

$$A_i(p, v)\dot{v} = B_i(p, v). \tag{5}$$

where:

$$\begin{aligned} p &= [\xi_1 \ \ \xi_2 \ \ \dots \ \ \xi_n \ \ \xi_p]^T, \\ v &= [\dot{\xi}_1 \ \ \dot{\xi}_2 \ \ \dots \ \ \dot{\xi}_n \ \ \dot{\xi}_p]^T, \\ A_i &= 2{\pounds_i}^T[0_{3\times3(i-1)} \ \ I_{3\times3} \ \ 0_{3\times3(n-i)} \ \ -I_{3\times3}], \\ B_i &= -2\dot{\pounds}_i^T\dot{\pounds}_i. \end{aligned} \tag{6}$$

Then, the constraint forces of all the ropes can be calculated by [26]:

$$\mathbb{T} = M^{1/2}(AM^{-1/2})^+(B - 2\alpha\dot{\varrho} - \beta^2\varrho - A\ddot{\chi}). \tag{7}$$

where, $\mathbb{T} = [\mathbb{T}_1, \mathbb{T}_2, \dots, \mathbb{T}_n, \sum_{i=1}^{n} \mathbb{T}_i]^T$, $\ddot{\chi}$ is the unconstrained acceleration of the cooperative transport system, $(\cdot)^+$ denotes the Moore-Penrose pseudo inverse, $\alpha$ and $\beta$ are feedback gains, and finally $M \in \mathbb{R}^{(n+1)\times(n+1)}$ is:

$$M = \begin{bmatrix} m_1 I_{3\times3} & 0_{3\times3} & \dots & 0_{3\times3} & 0_{3\times3} \\ 0_{3\times3} & m_2 I_{3\times3} & \dots & 0_{3\times3} & 0_{3\times3} \\ 0_{3\times3} & 0_{3\times3} & \dots & m_n I_{3\times3} & 0_{3\times3} \\ 0_{3\times3} & 0_{3\times3} & \ddots & 0_{3\times3} & m_L I_{3\times3} \end{bmatrix}. \tag{8}$$

*Remark 1:* The tensions obtained in (7) were calculated for simulation purposes. These tension forces cannot be measured directly; therefore, a nonlinear disturbance observer will estimate these forces in later sections.

## III. COOPERATIVE FLIGHT FORMATION

In this paper, the cooperative transport system is considered as a flight formation of a multi-agent system since it can provide advantages such as uniform payload distribution, collision avoidance, and payload oscillation reduction. Therefore, this paper employs graph theory for the flight formation of the cooperative transport system.

### A. GRAPH THEORY

Graph theory is extensively used for a communication network in multi-agent systems [13]. Consider a group of $n$ agents communicating with their neighbors described by the graph $G = (V, E)$, where $V$ and $E$ represent the nodes and edges, respectively. An edge $(V_i, V_j)$ means that agent $i$ can access the information of agent $j$ and vice versa. The adjacency matrix of a graph is defined as $A$, whose elements are $a_{ij} > 0$ if $(V_i, V_j) \in E$ and $a_{ij} = 0$ otherwise. The degree matrix is defined as $D = diag(d_1, \dots d_n) \in R^{n\times n}$ with $d_i = \sum_{j=1}^{n} a_{ij}$. Then, the Laplacian matrix can be expressed as $L = D - A$. In multi-agent systems, one agent is called the leader, and the other agents are called followers; the diagonal matrix of the leader is defined as $B = diag(b_1, \dots b_n)$, where $b_i > 0$ if agent $i$ can access the information of the leader; otherwise $b_i = 0$.

*Assumption 1:* The network is considered to be directed for flight formation of the cooperative transport system.

*Lemma 1:* According to the assumption 1, all eigenvalues of the matrix L + B have positive real parts [46].

For the flight formation of the cooperative transport system, a point is selected as the formation center, which is considered as the leader agent of the group. Under this premise and based on research works [12], [26], in this paper the payload is considered as a virtual leader, which is represented

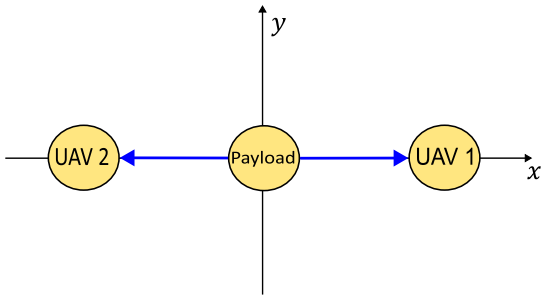


**FIGURE 2.** Communication topology of the desired formation pattern.

by the subscript $L$, and the quadcopters as followers, which are represented by the subscript $i$. Thereby, a desired formation pattern is established as a straight line shape in the $xy$-plane, such that the quadcopters are in a symmetric position with respect to the payload position. The Fig. 2 illustrates the graphical communication of the desired formation pattern for the cooperative transport system.

Next, the formation error and its derivative for the $i$-th quadcopter are defined as follows:

$$\begin{aligned} e_i^{\xi} &= \sum_{j=1}^{n} a_{ij}(\xi_j - \xi_i - (\Delta_j - \Delta_i)) + b_i(\xi_L^d - \xi_i + \Delta_i), \\ e_i^{V} &= \sum_{j=1}^{n} a_{ij}(V_j - V_i) + b_i(V_L^d - V_i). \end{aligned} \tag{9}$$

where $\xi_i = [x_i, y_i, z_i]^T$ and $V_i = [\dot{x}_i, \dot{y}_i, \dot{z}_i]^T$ represent the position and velocity of the $i$-th quadcopter. $\xi_L^d = [x_L^d, y_L^d, z_L^d]^T$ and $V_L^d = [\dot{x}_L^d, \dot{y}_L^d, \dot{z}_L^d]^T$ represent the desired position and velocity for the virtual leader. $\Delta_i = [\Delta_{xi}, \Delta_{yi}, \Delta_{zi}]^T$ represents the expected relative formation distance between the $i$-th quadcopter and the virtual leader. Expressing (9) in its general form for the cooperative transport system is given as follows:

$$\begin{aligned} E_X &= (L + B \otimes I_3)[X - \overline{X}_L - \Delta]^T, \\ E_V &= (L + B \otimes I_3)[V - \overline{V}_L]^T. \end{aligned} \tag{10}$$

where $\otimes$ denotes the Kronecker product, $X = [\xi_1, \ldots \xi_n]^T$ and $V = [\dot{\xi}_1, \ldots \dot{\xi}_n]^T$ represent the position and velocity vector of the agents, respectively, and finally, $\overline{X}_L, \overline{V}_L, \Delta$ is defined as:

$$\begin{aligned} \overline{X}_L &= ([1, \ldots, 1]^T)_{n\times 1} \otimes [x_L^d, y_L^d, z_L^d]^T, \\ \overline{V}_L &= ([1, \ldots, 1]^T)_{n\times 1} \otimes [\dot{x}_L^d, \dot{y}_L^d, \dot{z}_L^d]^T, \\ \Delta &= ([1, \ldots, 1]^T)_{n\times 1} \otimes [\Delta_i]. \end{aligned} \tag{11}$$

### B. CONTROL OBJECTIVE

The control objective is:

- Transport the payload safely with minimal oscillation.
- Achieve the desired formation pattern and maintain it throughout the cooperative transport task.
- Guarantee the stability of the formation errors at the origin at a fixed time $T_f$, even in the presence of lumped disturbances, i.e.

$$\begin{aligned} &\lim_{t\to T_f} e_i^{\xi} = 0, \\ &\lim_{t\to T_f} (\xi_i - \xi_L) = \Delta_i, \\ &\lim_{t\to T_f} (\xi_i - \xi_j) = (\Delta_i - \Delta_j). \end{aligned} \tag{12}$$

## IV. PROPOSED CONTROL DESIGN

In this section, control inputs are designed for the cooperative transport of a payload using two quadcopters as underactuated mechanical systems, i.e., only four control inputs are designed for each quadcopter. The proposed controller structure is divided into two subsystems: fully actuated ($U_{1i}$, $U_{4i}$) and underactuated ($U_{2i}$, $U_{3i}$). An integral sliding mode adaptive control strategy is proposed for the fully actuated subsystem, and for the underactuated subsystem, an adaptive control strategy based on the combination of Backstepping and sliding mode is proposed. The control parameters of the sliding surfaces of both subsystems are adaptively tuned with a neural network that is trained by the backpropagation algorithm to minimize the errors of the cooperative transport system. To improve the performance of the proposed controller, a disturbance observer is incorporated to estimate the disturbances, including rope tensions that dramatically affect the quadcopter dynamics.

### A. NONLINEAR DISTURBANCE OBSERVER

Due to the presence of unmeasurable states in the cooperative transport system, a nonlinear disturbance observer is incorporated into the controller to estimate and compensate for lumped disturbances. The equation (2) can be written as the following nonlinear state space form:

$$\begin{aligned} \dot{X}_{\mathcal{T}} &= X_{\mathcal{T}+1}, \\ \dot{X}_{\mathcal{T}+1} &= f(X) + g(X)U + d(t). \end{aligned} \tag{13}$$

where $X_{\mathcal{T}} = [x, \dot{x}, y, \dot{y}, z, \dot{z}, \phi, \dot{\phi}, \theta, \dot{\theta}, \psi, \dot{\psi}]^T$ is the vector of states, $U = [U_{1i}, U_{2i}, U_{3i}, U_{4i}]^T$ are the control inputs, $f$ and $g$ are two known, real, nonlinear smooth functions of $X_{\mathcal{T}}$, and $d(t)$ are the unknown lumped disturbances.

*Assumption 2:* The disturbances $d(t)$ are limited by $d(t) \leq D$, $t > 0$, and D is a positive definite constant.

*Assumption 3:* The derivative of $d(t)$ is bounded and satisfies $\lim_{t\to\infty} \dot{d}(t) = 0$.

Estimation of the disturbances $\widehat{d}(t)$ are calculated using the nonlinear disturbance observer according to the following algorithm developed in [47]:

$$\begin{aligned} \dot{\Pi} &= -\lambda\Pi - \lambda[\lambda\dot{\Gamma} + f(X) + g(X)U], \\ \widehat{d}(t) &= \Pi + \lambda\dot{\Gamma}, \end{aligned} \tag{14}$$

$\Pi \in \mathbb{R}^6$ and $\lambda = \lambda I_{6\times 6} \in \mathbb{R}^{6\times 6}$ denote the internal state vector and the observer gain matrix, respectively, and $\Gamma = [x, y, z, \phi, \theta, \psi]^T$ are the states.

The estimation error of the disturbances and its time derivative are defined as follows:

$$\widetilde{d}(t) = d(t) - \widehat{d}(t),$$

$$\dot{\tilde{d}}\,(t) = \dot{d}(t) - \dot{\hat{d}}\,(t). \tag{15}$$

Substitute (13) and (14) into (15), the following expression is obtained:

$$\begin{aligned}\dot{\tilde{d}}\,(t) &= \dot{d}(t) - (\dot{\Pi} - \lambda\dot{\Gamma}) \\ &= \dot{d}(t) - (-\lambda\Pi - \lambda[\lambda\dot{\Gamma} + f(X) + g(X)U] \\ &\quad - \lambda(f(X) + g(X)U + d(t))) \\ &= \dot{d}(t) - (-\lambda\Pi - \lambda^2\dot{\Gamma} + \lambda d(t)) \\ &= \dot{d}(t) - (-\lambda\hat{d}(t) + \lambda d(t)) \\ &= \dot{d}(t) - \lambda\tilde{d}(t). \end{aligned} \tag{16}$$

*Lemma 2:* According to assumptions 2 and 3, the disturbances estimate $\hat{d}(t)$ of the designed observer in (14) can track the lumped disturbances if the observer gains are properly selected $\lambda > 0$ [47]. The equation (16) can be rewritten as:

$$\dot{\tilde{d}}\,(t) + \lambda\tilde{d}(t) = 0,$$

therefore, the estimation error of the disturbances $\tilde{d}(t)$ is globally asymptotically stable.

### B. CONTROL DESIGN FOR THE FULLY ACTUATED SUBSYSTEM

The fully actuated control subsystem for the $i$-th quadcopter is formed by the inputs $[U_{1i}, U_{4i}]^T$ and outputs $[z_i, \psi_i]^T$. Therefore, an integral sliding mode adaptive control strategy is proposed.

The fully actuated control subsystem errors are defined as:

$$\begin{aligned} e_i^z &= \sum_{j=1}^{n} a_{ij}(z_j - z_i - \Delta_{jiz}) + b_i(z_L^d - z_i + \Delta_{iz}), \\ e_i^\psi &= \psi_i^d - \psi_i. \end{aligned} \tag{17}$$

The time derivative of (17) is given by:

$$\begin{aligned} \dot{e}_i^z &= \sum_{j=1}^{n} a_{ij}(\dot{z}_j - \dot{z}_i) + b_i(\dot{z}_L^d - \dot{z}_i), \\ \dot{e}_i^\psi &= \dot{\psi}_i^d - \dot{\psi}_i. \end{aligned} \tag{18}$$

The following sliding surfaces for the fully actuated control subsystem are introduced as:

$$\begin{aligned} s_{z_i} &= \dot{e}_i^z + \Xi_1 e_i^z + \Xi_2 \int_0^t e_i^z dt, \\ s_{\psi_i} &= \dot{e}_i^\psi + \Xi_3 e_i^\psi + \Xi_4 \int_0^t e_i^\psi dt. \end{aligned} \tag{19}$$

where the parameters $\Sigma_\sigma (\sigma = 1, \ldots, 4)$ are positive definite and will be tuned with a neural network later. The time derivative of (19) is given by:

$$\begin{aligned} \dot{s}_{z_i} &= \ddot{e}_i^z + \Xi_1 \dot{e}_i^z + \Xi_2 e_i^z, \\ \dot{s}_{\psi_i} &= \ddot{e}_i^\psi + \Xi_3 \dot{e}_i^\psi + \Xi_4 e_i^\psi. \end{aligned} \tag{20}$$

To design the control inputs, the following condition must be satisfied [34]:

$$\dot{s}_{z_i} = -\varepsilon_z \text{sign}(s_{z_i}) - \eta_z s_{z_i},$$

$$\dot{s}_{\psi_i} = -\varepsilon_\psi \text{sign}(s_{\psi_i}) - \eta_\psi s_{\psi_i}. \tag{21}$$

According to (20) and (21), the control inputs $U_{1i}$ and $U_{4i}$ for the $i$-th quadcopter are designed as follows:

$$\begin{cases} U_{1i} = \dfrac{cos\phi_i cos\theta_i}{m_{qi}}\Big[(b_i + \sum_{j=1}^{n} a_{ij})^{-1}(\Xi_1 \dot{e}_i^z + \Xi_2 e_i^z + b_i \ddot{z}_L^d \\ \qquad + \sum_{j=1}^{n} a_{ij}\ddot{y}_j + \varepsilon_z \text{sign}(s_{z_i}) + \eta_z s_{z_i}) + g + \hat{T}_z - \hat{\delta}_z(t)\Big], \\ U_{4i} = \dfrac{J_{zi}}{\kappa}\Big[\Xi_3 \dot{e}_i^\psi + \Xi_4 e_i^\psi + \ddot{\psi}_i^d + \varepsilon_\psi \text{sign}(s_{\psi_i}) + \eta_\psi s_{\psi_i} \\ \qquad - \dfrac{(J_{xi} - J_{yi})}{J_{zi}}\dot{\phi}_i\dot{\theta}_i - \hat{\delta}_\psi\Big]. \end{cases} \tag{22}$$

where $\varepsilon_\rho > 0$ and $\eta_\rho > 0 (\rho = z, \psi)$ are the switching parameters.

*Remark 2:* To solve the chattering problem, in the control laws designed in (22), the *sign*(.) function is substituted by the *tanh*(.) function.

*Theorem 1:* The control inputs designed in (22) with the nonlinear disturbance observer in (14) guarantee the asymptotic stability of the cooperative transport system such that the output states $[z_i, \psi_i]^T$ converge to their desired values in a finite time. Furthermore the errors in (17) converge to zero in a finite time.

*Proof 1:* To demonstrate the stability, the following candidate Lyapunov functions are defined as:

$$\begin{bmatrix} V_i^z \\ V_i^\psi \end{bmatrix} = \begin{bmatrix} \frac{1}{2}s_{z_i}^2 + \frac{1}{2}\tilde{d}_z^{\,2} \\ \frac{1}{2}s_{\psi_i}^2 + \frac{1}{2}\tilde{d}_\psi^{\,2} \end{bmatrix}. \tag{23}$$

The time derivative of (23) and substituting (16), (19), (20) and (22), the following expressions are obtained:

$$\begin{bmatrix} \dot{V}_i^z \\ \dot{V}_i^\psi \end{bmatrix} = \begin{bmatrix} -\varepsilon_z |s_{z_i}| - \eta_z s_{z_i}^2 - \lambda\tilde{d}_z^{\,2} \\ -\varepsilon_\psi |s_{\psi_i}| - \eta_\psi s_{\psi_i}^2 - \lambda\tilde{d}_\psi^{\,2} \end{bmatrix} \leq 0. \tag{24}$$

*Remark 3:* From (24), it can be concluded that the fully actuated control subsystem guarantees the asymptotic stability of the cooperative transport system. Therefore, Theorem 1 has been verified.

*Remark 4:* The sliding surfaces in (22) have four design parameters $\Xi_1, \Xi_2, \Xi_3, \Xi_4$ and two switching parameters $\varepsilon_z, \varepsilon_\psi$. These parameters are adaptively tuned with a neural network that is trained by the backpropagation algorithm to minimize the errors of the fully actuated control subsystem.

Next, the control parameters of the sliding surface $s_{z_i}$ are designed in the following steps:

1) First, the error function is defined as follows:

$$E_z = \frac{1}{2}[e_i^z]^2. \tag{25}$$

2) By employing the steepest descent method [48], the following adaptive equations are obtained:

$$\begin{aligned}\varepsilon_z &= \varepsilon_{z,0} - \omega_z \frac{\partial E_z}{\partial \varepsilon_z},\\ \Xi_1 &= \Xi_{1,0} - \omega_z \frac{\partial E_z}{\partial \Xi_1},\\ \Xi_2 &= \Xi_{2,0} - \omega_z \frac{\partial E_z}{\partial \Xi_2}.\end{aligned} \tag{26}$$

where $\omega_z$ is the learning rate, $\varepsilon_{z,0}$ and $\Xi_{\sigma,0}(\sigma = 1, 2)$ are the initial values of $\varepsilon_z$ and $\Xi_\sigma(\sigma = 1, 2)$, respectively.

3) Using the chain rule for partial derivatives, the following equations are obtained:

$$\begin{aligned}\frac{\partial E_z}{\partial \varepsilon_z} &= \frac{\partial E_z}{\partial z}\frac{\partial z}{\partial U_1}\frac{\partial U_1}{\partial \varepsilon_z} = \frac{-m_q e_i^z}{cos(\phi)cos(\theta)}\tanh(s_z),\\ \frac{\partial E_z}{\partial \Xi_1} &= \frac{\partial E_z}{\partial z}\frac{\partial z}{\partial U_1}\frac{\partial U_1}{\partial s_z}\frac{\partial s_z}{\partial \Xi_1}\\ &= \frac{-m_q (e_i^z)^2}{cos(\phi)cos(\theta)}\left(\eta_z + \frac{4e^{-2s_z}\varepsilon_z}{(1+e^{-2s_z})^2}\right),\\ \frac{\partial E_z}{\partial \Xi_2} &= \frac{\partial E_z}{\partial z}\frac{\partial z}{\partial U_1}\frac{\partial U_1}{\partial s_z}\frac{\partial s_z}{\partial \Xi_2}\\ &= \frac{-m_q e_i^z \int_0^t e_i^z\, dt}{cos(\phi)cos(\theta)}\left(\eta_z + \frac{4e^{-2s_z}\varepsilon_z}{(1+e^{-2s_z})^2}\right).\end{aligned} \tag{27}$$

4) Substituting (27) into (26), the control parameters of the sliding surface $s_{zi}$ are given as:

$$\begin{aligned}\varepsilon_z &= \varepsilon_{z,0} + \omega_z\left[\frac{m_q e_i^z}{cos(\phi)cos(\theta)}\tanh(s_z)\right],\\ \Xi_1 &= \Xi_{1,0} + \omega_z\left[\frac{m_q (e_i^z)^2}{cos(\phi)cos(\theta)}\left(\eta_z + \frac{4e^{-2s_z}\varepsilon_z}{(1+e^{-2s_z})^2}\right)\right],\\ \Xi_2 &= \Xi_{2,0} + \omega_z\left[\frac{m_q e_i^z \int_0^t e_i^z\, dt}{cos(\phi)cos(\theta)}\left(\eta_z + \frac{4e^{-2s_z}\varepsilon_z}{(1+e^{-2s_z})^2}\right)\right].\end{aligned} \tag{28}$$

By following the same procedure as above (step 1 to step 4) the control parameters of the sliding surface $s_\psi$ are obtained:

$$\begin{aligned}\varepsilon_\psi &= \varepsilon_{\psi,0} + \omega_\psi\left[\frac{J_z e_i^\psi}{\kappa}\tanh(s_\psi)\right],\\ \Xi_3 &= \Xi_{3,0} + \omega_\psi\left[\frac{J_z (e_i^\psi)^2}{\kappa}\left(\eta_\psi + \frac{4e^{-2s_\psi}\varepsilon_\psi}{(1+e^{-2s_\psi})^2}\right)\right],\\ \Xi_4 &= \Xi_{4,0} + \omega_\psi\left[\frac{J_z e_i^\psi \int_0^t e_i^\psi\, dt}{\kappa}\left(\eta_\psi + \frac{4e^{-2s_\psi}\varepsilon_\psi}{(1+e^{-2s_\psi})^2}\right)\right].\end{aligned} \tag{29}$$

### C. CONTROL DESIGN FOR THE UNDERACTUATED SUBSYSTEM

The underactuated control subsystem for the $i$-th quadcopter is formed by the inputs $[U_{2i}, U_{3i}]^T$ and outputs $[x_i, y_i, \phi_i, \theta_i]^T$. Clearly, it is impossible to design a control strategy for each output. Therefore, an adaptive control strategy based on the combination of Backstepping and sliding mode control techniques is proposed due to its good robustness characteristics to control underactuated mechanical systems.

The underactuated control subsystem errors are defined as:

$$\begin{aligned}e_i^x &= \sum_{j=1}^{n} a_{ij}(x_j - x_i - \Delta_{jix}) + b_i(x_L^d - x_i + \Delta_{ix}),\\ e_i^y &= \sum_{j=1}^{n} a_{ij}(y_j - y_i - \Delta_{jiy}) + b_i(y_L^d - y_i + \Delta_{iy}),\\ e_i^\phi &= \phi_i^d - \phi_i,\\ e_i^\theta &= \theta_i^d - \theta_i.\end{aligned} \tag{30}$$

The first time derivative of (30) is given as:

$$\begin{aligned}\dot{e}_i^x &= \sum_{j=1}^{n} a_{ij}(\dot{x}_j - \dot{x}_i) + b_i(\dot{x}_L^d - \dot{x}_i),\\ \dot{e}_i^y &= \sum_{j=1}^{n} a_{ij}(\dot{y}_j - \dot{y}_i) + b_i(\dot{y}_L^d - \dot{y}_i),\\ \dot{e}_i^\phi &= \dot{\phi}_i^d - \dot{\phi}_i,\\ \dot{e}_i^\theta &= \dot{\theta}_i^d - \dot{\theta}_i.\end{aligned} \tag{31}$$

Then, the first Lyapunov candidate function for $e_i^\phi$ and $e_i^\theta$ are chosen as:

$$\begin{aligned}V_{1i}^\phi &= \frac{1}{2}{e_i^\phi}^2,\\ V_{1i}^\theta &= \frac{1}{2}{e_i^\theta}^2.\end{aligned} \tag{32}$$

Deriving the first Lyapunov candidate functions (32) and substituting the time derivative of the errors $e_{1i}^\phi$ and $e_{1i}^\theta$ gives the following expression:

$$\begin{aligned}\dot{V}_{1i}^\phi &= e_i^\phi \dot{e}_i^\phi = e_i^\phi(\dot{\phi}_i^d - \dot{\phi}_i),\\ \dot{V}_{1i}^\theta &= e_i^\theta \dot{e}_i^\theta = e_i^\theta(\dot{\theta}_i^d - \dot{\theta}_i).\end{aligned} \tag{33}$$

In order to stabilize $e_{1i}^\phi$ and $e_{1i}^\theta$, the following virtual control inputs are introduced as follows: [49]:

$$\begin{aligned}\dot{\phi}_i^* &= \dot{\phi}_i^d + k_{e_\phi} e_i^\phi + s_{\phi_i},\\ \dot{\theta}_i^* &= \dot{\theta}_i^d + k_{e_\theta} e_i^\theta + s_{\theta_i}.\end{aligned} \tag{34}$$

where $k_{e_\phi}$ y $k_{e_\theta}$ are positive definite constants. Inspired by [36], [50], the following sliding surfaces are proposed for the underactuated control subsystem as follows:

$$\begin{aligned}s_{\phi_i} &= c_1\dot{e}_i^y + c_2 e_i^y + c_3\left|e_i^y\right|^{\alpha_y}\operatorname{sgn}(e_i^y)\\ &\quad + \dot{e}_i^\phi + c_4 e_i^\phi + c_5\left|e_i^\phi\right|^{\alpha_\phi}\operatorname{sgn}(e_i^\phi),\\ s_{\theta_i} &= c_6\dot{e}_i^x + c_7 e_i^x + c_8\left|e_i^x\right|^{\alpha_x}\operatorname{sgn}(e_i^x)\\ &\quad + \dot{e}_i^\theta + c_9 e_i^\theta + c_{10}\left|e_i^\theta\right|^{\alpha_\theta}\operatorname{sgn}(e_i^\theta).\end{aligned} \tag{35}$$

The coefficients of the sliding surfaces in (35) are obtained using the Hurwitz stability analysis [34], where $c_1 = -\Xi_5 m_{qi}/(U_{1i}cos\psi_i)$, $c_2 = -\Xi_6 m_{qi}/(U_{1i}cos\psi_i)$, $c_3 = \Xi_7$, $c_4 = \Xi_8$, $c_5 = \Xi_9$, $c_6 = \Xi_{10} m_{qi}/(U_{1i}cos\phi_i cos\psi_i)$, $c_7 = \Xi_{11} m_{qi}/(U_{1i}cos\phi cos\psi)$, $c_8 = \Xi_{12}$, $c_9 = \Xi_{13}$, $c_{10} = \Xi_{14}$.

The parameters $\Xi_\sigma(\sigma = 5, \ldots, 14)$ are positive definite and will be tuned with a neural network later, $\alpha_\rho(\rho = x, y, \phi, \theta)$ are positive definite constants. The time derivative of the (35) is as follows:

$$\begin{aligned}
\dot{s}_{\phi_i} &= c_1\ddot{e}_i^y + c_2\dot{e}_i^y + c_3\alpha_y \left|e_i^y\right|^{\alpha_y - 1}\dot{e}_i^y + \ddot{e}_i^\phi \\
&\quad + c_4\dot{e}_i^\phi + c_5\alpha_\phi \left|e_i^\phi\right|^{\alpha_\phi - 1}\dot{e}_i^\phi, \\
\dot{s}_{\theta_i} &= c_6\ddot{e}_i^x + c_7\dot{e}_i^x + c_8\alpha_x \left|e_i^x\right|^{\alpha_x - 1}\dot{e}_i^x + \ddot{e}_i^\theta \\
&\quad + c_9\dot{e}_i^\theta + c_{10}\alpha_\theta \left|e_i^\theta\right|^{\alpha_\theta - 1}\dot{e}_i^\theta.
\end{aligned} \tag{36}$$

Next, the second Lyapunov candidate function are chosen as:

$$\begin{aligned}
V_{2i}^\phi &= \frac{1}{2}{e_i^\phi}^2 + \frac{1}{2}s_{\phi_i}^2, \\
V_{2i}^\theta &= \frac{1}{2}{e_i^\theta}^2 + \frac{1}{2}s_{\theta_i}^2.
\end{aligned} \tag{37}$$

The time derivative of the second Lyapunov candidate function (37), and substituting (34) and (36) gives:

$$\begin{aligned}
\dot{V}_{2i}^\phi &= -k_{e_\phi}{e_i^\phi}^2 - s_{\phi_i}e_i^\phi + s_{\phi_i}\big(c_1\ddot{e}_i^y + c_2\dot{e}_i^y + \ddot{e}_i^\phi \\
&\quad + c_3\alpha_y \left|e_i^y\right|^{\alpha_y - 1}\dot{e}_i^y + c_4\dot{e}_i^\phi + c_5\alpha_\phi \left|e_i^\phi\right|^{\alpha_\phi - 1}\dot{e}_i^\phi\big), \\
\dot{V}_{2i}^\theta &= -k_{e_\theta}{e_i^\theta}^2 - s_{\theta_i}e_i^\theta + s_{\theta_i}\big(c_6\ddot{e}_i^x + c_7\dot{e}_i^x + \ddot{e}_i^\theta \\
&\quad + c_8\alpha_x \left|e_i^x\right|^{\alpha_x - 1}\dot{e}_i^x + c_9\dot{e}_i^\theta + c_{10}\alpha_\theta \left|e_i^\theta\right|^{\alpha_\theta - 1}\dot{e}_i^\theta\big).
\end{aligned} \tag{38}$$

According to (38), the control inputs $U_{2i}$ and $U_{3i}$ for the $i$-th quadcopter are designed as follows:

$$\begin{cases}
U_{2i} = \dfrac{J_{xi}}{\varsigma}\Big[ -e_i^\phi + k_{s_\phi}s_{\phi_i} + c_1\Big(b_i\ddot{y}_L^d - (\upsilon_{yi} - \widehat{T}_y \\
\quad + \widehat{\delta}_y(t))(\sum_{j=1}^{n} a_{ij} + b_i) + \sum_{j=1}^{n} a_{ij}\ddot{y}_j\Big) + c_2\dot{e}_i^y \\
\quad + c_3\alpha_y \left|e_i^y\right|^{\alpha_y - 1}\dot{e}_i^y + \ddot{\phi}_{1i}^d + c_4\dot{e}_i^\phi + c_5\alpha_\phi \left|e_i^\phi\right|^{\alpha_\phi - 1} \\
\quad \times \dot{e}_i^\phi + \varepsilon_\phi sign(s_{\phi_i}) + \eta_\phi s_{\phi_i} - \dfrac{J_{yi} - J_{zi}}{J_{xi}}\dot{\theta}_i\dot{\psi}_i \\
\quad + \dfrac{J_{ri}}{J_{xi}}\dot{\theta}_i\Omega_i - \widehat{\delta}_\phi\Big], \\
U_{3i} = \dfrac{J_{yi}}{\varsigma}\Big[ -e_i^\theta + k_{s_\theta}s_{\theta_i} + c_6\Big(b_i\ddot{x}_L^d - (\upsilon_{xi} - \widehat{T}_x \\
\quad + \widehat{\delta}_x(t))(\sum_{j=1}^{n} a_{ij} + b_i) + \sum_{j=1}^{n} a_{ij}\ddot{x}_j\Big) + c_7\dot{e}_i^x \\
\quad + c_8\alpha_x \left|e_i^x\right|^{\alpha_x - 1}\dot{e}_i^x + \ddot{\theta}_{1i}^d + c_9\dot{e}_i^\theta + c_{10}\alpha_\theta \left|e_i^\theta\right|^{\alpha_\theta - 1} \\
\quad \times \dot{e}_i^\theta + \varepsilon_\theta sign(s_{\theta_i}) + \eta_\theta s_{\theta_i} - \dfrac{J_{zi} - J_{xi}}{J_{yi}}\dot{\phi}_i\dot{\psi}_i \\
\quad + \dfrac{J_{ri}}{J_{yi}}\dot{\phi}_i\Omega_i - \widehat{\delta}_\theta\Big].
\end{cases} \tag{39}$$

where, $\upsilon_{xi} = (c\phi_i s\theta_i c\psi_i + s\phi_i s\psi_i)\,U_{1i}$ and $\upsilon_{yi} = (c\phi_i s\theta_i s\psi_i - s\phi_i c\psi_i)\,U_{1i}$, $k_{s_\phi} > 0, k_{s_\theta} > 0$ are positive definite constants, and the coefficients $\varepsilon_\rho > 0$ and $\eta_\rho > 0$ $(\rho = \phi, \theta)$ are the switching parameters.

*Remark 5:* To solve the chattering problem, in the control laws designed in (39), the *sign*(.) function is substituted by the *tanh*(.) function.

*Theorem 2:* The control inputs designed in (39) with the nonlinear disturbance observer in (14) guarantee the asymptotic stability of the cooperative transport system such that the output states $[x_i, y_i, \phi_i, \theta_i]^T$ converge to their desired values in a finite time. Furthermore the errors in (30) converge to zero in a finite time.

*Proof 2:* To demonstrate the stability, the following candidate Lyapunov functions are defined as:

$$\begin{bmatrix} V_i^\phi \\ V_i^\theta \end{bmatrix} = \begin{bmatrix} \frac{1}{2}{e_i^\phi}^2 + \frac{1}{2}s_{\phi_i}^2 + \frac{1}{2}\widetilde{d}_\phi^2 + \frac{1}{2}\widetilde{d}_y^2 \\ \frac{1}{2}{e_i^\theta}^2 + \frac{1}{2}s_{\theta_i}^2 + \frac{1}{2}\widetilde{d}_\theta^2 + \frac{1}{2}\widetilde{d}_x^2 \end{bmatrix}. \tag{40}$$

The time derivative of (40) and substituting (16), (33), (38) and (39), the following expressions are obtained:

$$\begin{aligned}
\begin{bmatrix} \dot{V}_i^\phi \\ \dot{V}_i^\theta \end{bmatrix} &= \begin{bmatrix} -k_{e_\phi}{e_i^\phi}^2 - k_{s_\phi}s_{\phi_i}^2 - \varepsilon_\phi|s_\phi| - \lambda_\phi\widetilde{d}_\phi^2 - \lambda_y\widetilde{d}_y^2 \\ -k_{e_\theta}{e_i^\theta}^2 - k_{s_\theta}s_{\theta_i}^2 - \varepsilon_\theta|s_\theta| - \lambda_\theta\widetilde{d}_\theta^2 - \lambda_x\widetilde{d}_x^2 \end{bmatrix} \\
&\leq 0.
\end{aligned} \tag{41}$$

*Remark 6:* From (41), it can be concluded that the underactuated control subsystem guarantees the asymptotic stability of the cooperative transport system. Therefore, Theorem 2 has been verified.

*Remark 7:* The sliding surfaces in (39) have ten design parameters $\Xi_5$, $\Xi_6$, $\Xi_7$, $\Xi_8$, $\Xi_9$, $\Xi_{10}$, $\Xi_{11}$, $\Xi_{12}$, $\Xi_{13}$, $\Xi_{14}$ and two switching parameters $\varepsilon_\phi$, $\varepsilon_\theta$. These parameters are adaptively tuned with a neural network that is trained by the backpropagation algorithm to minimize the errors of the underactuated control subsystem.

Next, the control parameters of the sliding surface $s_{\phi_i}$ are designed in the following steps:

1) First, the error function is defined as follows:

$$E_y = \frac{1}{2}\big[e_i^y\big]^2. \tag{42}$$

2) By employing the steepest descent method [48], the following adaptive equations are obtained:

$$\begin{cases}
\varepsilon_\phi = \varepsilon_{\phi,0} - \omega_\phi\dfrac{\partial E_y}{\partial \varepsilon_\phi}, \\
\Xi_5 = \Xi_{5,0} - \omega_\phi\dfrac{\partial E_y}{\partial \Xi_1}, \\
\Xi_6 = \Xi_{6,0} - \omega_\phi\dfrac{\partial E_y}{\partial \Xi_2}, \\
\Xi_7 = \Xi_{7,0} - \omega_\phi\dfrac{\partial E_y}{\partial \Xi_3}, \\
\Xi_8 = \Xi_{8,0} - \omega_\phi\dfrac{\partial E_y}{\partial \Xi_4}, \\
\Xi_9 = \Xi_{9,0} - \omega_\phi\dfrac{\partial E_y}{\partial \Xi_5}.
\end{cases} \tag{43}$$

where $\omega_\phi$ is the learning rate, $\varepsilon_{\phi,0}$ and $\Xi_{\sigma,0}(\sigma = 5,\ldots,9)$ are the initial values of $\varepsilon_\phi$ and $\Xi_\sigma(\sigma = 5,\ldots,9)$, respectively.

3) Using the chain rule for partial derivatives, the following equations are obtained:

$$\begin{aligned}
\frac{\partial E_y}{\partial \varepsilon_\phi} &= \frac{\partial E_y}{\partial y}\frac{\partial y}{\partial U_2}\frac{\partial U_2}{\partial \varepsilon_\phi} = \frac{-J_x e_i^y}{\varsigma}\tanh(s_\phi),\\
\frac{\partial E_y}{\partial \Xi_5} &= \frac{\partial E_y}{\partial y}\frac{\partial y}{\partial U_2}\frac{\partial U_2}{\partial s_\phi}\frac{\partial s_\phi}{\partial \Xi_5}\\
&= \frac{J_x e_i^y \dot{e}_i^y m_q}{\varsigma(cos\psi U_1)}\left(\eta_\phi + \frac{4e^{-2s_\phi}\varepsilon_\phi}{(1+e^{-2s_\phi})^2}\right),\\
\frac{\partial E_y}{\partial \Xi_6} &= \frac{\partial E_y}{\partial y}\frac{\partial y}{\partial U_2}\frac{\partial U_2}{\partial s_\phi}\frac{\partial s_\phi}{\partial \Xi_6}\\
&= \frac{J_x (e_i^y)^2 m_q}{\varsigma(cos\psi U_1)}\left(\eta_\phi + \frac{4e^{-2s_\phi}\varepsilon_\phi}{(1+e^{-2s_\phi})^2}\right),\\
\frac{\partial E_y}{\partial \Xi_7} &= \frac{\partial E_y}{\partial y}\frac{\partial y}{\partial U_2}\frac{\partial U_2}{\partial s_\phi}\frac{\partial s_\phi}{\partial \Xi_7}\\
&= \frac{-J_x e_i^y \left|e_i^y\right|^{\alpha_y}\mathrm{sgn}(e_i^y)}{\varsigma}\left(\eta_\phi + \frac{4e^{-2s_\phi}\varepsilon_\phi}{(1+e^{-2s_\phi})^2}\right),\\
\frac{\partial E_y}{\partial \Xi_8} &= \frac{\partial E_y}{\partial y}\frac{\partial y}{\partial U_2}\frac{\partial U_2}{\partial s_\phi}\frac{\partial s_\phi}{\partial \Xi_8}\\
&= \frac{-J_x e_i^y e_i^\phi}{\varsigma}\left(\eta_\phi + \frac{4e^{-2s_\phi}\varepsilon_\phi}{(1+e^{-2s_\phi})^2}\right),\\
\frac{\partial E_y}{\partial \Xi_9} &= \frac{\partial E_y}{\partial y}\frac{\partial y}{\partial U_2}\frac{\partial U_2}{\partial s_\phi}\frac{\partial s_\phi}{\partial \Xi_9}\\
&= \frac{-J_x e_i^y \left|e_i^\phi\right|^{\alpha_\phi}\mathrm{sgn}(e_i^\phi)}{\varsigma}\left(\eta_\phi + \frac{4e^{-2s_\phi}\varepsilon_\phi}{(1+e^{-2s_\phi})^2}\right).
\end{aligned} \tag{44}$$

4) Substituting equation (44) into (43), the control parameters of the sliding surface $s_\phi$ are given as:

$$\begin{aligned}
\varepsilon_\phi &= \varepsilon_{\phi,0} + \omega_\phi\left[\frac{J_x e_i^y}{\varsigma}\tanh(s_\phi)\right],\\
\Xi_5 &= \Xi_{5,0} - \omega_\phi\left[\frac{J_x e_i^y \dot{e}_i^y m_q}{\varsigma(cos\psi U_1)}\left(\eta_\phi + \frac{4e^{-2s_\phi}\varepsilon_\phi}{(1+e^{-2s_\phi})^2}\right)\right],\\
\Xi_6 &= \Xi_{6,0} - \omega_\phi\left[\frac{J_x (e_i^y)^2 m_q}{\varsigma(cos\psi U_1)}\left(\eta_\phi + \frac{4e^{-2s_\phi}\varepsilon_\phi}{(1+e^{-2s_\phi})^2}\right)\right],\\
\Xi_7 &= \Xi_{7,0} + \omega_\phi\left[\frac{J_x e_i^y \left|e_i^y\right|^{\alpha_y}\mathrm{sgn}(e_i^y)}{\varsigma}\right.\\
&\qquad\left.\times\left(\eta_\phi + \frac{4e^{-2s_\phi}\varepsilon_\phi}{(1+e^{-2s_\phi})^2}\right)\right],\\
\Xi_8 &= \Xi_{8,0} + \omega_\phi\left[\frac{J_x e_i^y e_i^\phi}{\varsigma}\left(\eta_\phi + \frac{4e^{-2s_\phi}\varepsilon_\phi}{(1+e^{-2s_\phi})^2}\right)\right],\\
\Xi_9 &= \Xi_{9,0} + \omega_\phi\left[\frac{J_x e_i^y \left|e_i^\phi\right|^{\alpha_\phi}\mathrm{sgn}(e_i^\phi)}{\varsigma}\right.\\
&\qquad\left.\times\left(\eta_\phi + \frac{4e^{-2s_\phi}\varepsilon_\phi}{(1+e^{-2s_\phi})^2}\right)\right].
\end{aligned} \tag{45}$$

By following the same procedure as above (step 1 to step 4) the control parameters of the sliding surface $s_\theta$ are obtained:

$$\begin{aligned}
\varepsilon_\theta &= \varepsilon_{\theta,0} + \omega_\theta\left[\frac{J_y e_i^x}{\varsigma}\tanh(s_\theta)\right],\\
\Xi_{10} &= \Xi_{10,0} + \omega_\theta\left[\frac{J_y e_i^x \dot{e}_i^x m_q}{\varsigma(cos\phi cos\psi U_1)}\left(\eta_\theta + \frac{4e^{-2s_\theta}\varepsilon_\theta}{(1+e^{-2s_\theta})^2}\right)\right],\\
\Xi_{11} &= \Xi_{11,0} + \omega_\theta\left[\frac{J_y (e_i^x)^2 m_q}{\varsigma(cos\phi cos\psi U_1)}\left(\eta_\theta + \frac{4e^{-2s_\theta}\varepsilon_\theta}{(1+e^{-2s_\theta})^2}\right)\right],\\
\Xi_{12} &= \Xi_{12,0} + \omega_\theta\left[\frac{J_y e_i^x \left|e_i^x\right|^{\alpha_x}\mathrm{sgn}(e_i^x)}{\varsigma}\right.\\
&\qquad\left.\times\left(\eta_\theta + \frac{4e^{-2s_\theta}\varepsilon_\theta}{(1+e^{-2s_\theta})^2}\right)\right],\\
\Xi_{13} &= \Xi_{13,0} + \omega_\theta\left[\frac{J_y e_i^x e_i^\theta}{\varsigma}\left(\eta_\theta + \frac{4e^{-2s_\theta}\varepsilon_\theta}{(1+e^{-2s_\theta})^2}\right)\right],\\
\Xi_{14} &= \Xi_{14,0} + \omega_\theta\left[\frac{J_y e_i^x \left|e_i^\theta\right|^{\alpha_\theta}\mathrm{sgn}(e_i^\theta)}{\varsigma}\right.\\
&\qquad\left.\times\left(\eta_\theta + \frac{4e^{-2s_\theta}\varepsilon_\theta}{(1+e^{-2s_\theta})^2}\right)\right].
\end{aligned} \tag{46}$$

## V. RESULTS AND DISCUSSIONS

In this section, the results of numerical simulations are presented to validate the efficiency and performance of the proposed controller for the cooperative transport of a payload using two underactuated quadcopters. The physical parameters of the cooperative transport system and the parameters for the control design are presented in Appendix A, Tables 1-2. The initial position of the quadcopters is set as $\xi_1^0 = (1, 0.5, 0)$m, $\xi_2^0 = (-1, -0.5, 0)$m, and the initial position of the payload is set as $\xi_p^0 = (0, 0, 0)$m.

The desired formation pattern is set as a straight line shape so that the quadcopters are in a symmetric position with respect to the payload position, which is considered the virtual leader of the cooperative transport system. The desired formation distance for each quadcopter is chosen as $\Delta_1 = [1, 0, \sqrt{3}]^T$ y $\Delta_2 = [-1, 0, \sqrt{3}]^T$. Two cases with different scenarios for the reference trajectory of the virtual leader were analyzed and are presented below:

### A. CASE 1: WITHOUT DISTURBANCES

In this case, disturbances such as wind gusts and parametric uncertainties are not considered. The desired trajectory for the virtual leader is chosen as $\xi_L^d = [2.5\cos(0.2t), 2.5\sin(0.2t), 0.267 + 0.1t]^T$m. Assuming that the desired orientation for each quadcopter is equal to $\eta^d = [\phi^d, \theta^d, \psi^d]^T = [0, 0, 0]^T$rad.

The simulation results are presented in Figs. 3-8. In Fig. 3, a three-dimensional view of the cooperative transport of a payload following a helicoidal trajectory is illustrated, where it can be seen that the two quadcopters transport the payload safely and without oscillations.

The Fig. 4 display the temporal response of the position of the cooperative transport system, as can be observed that the quadcopters and the payload achieve the desired formation

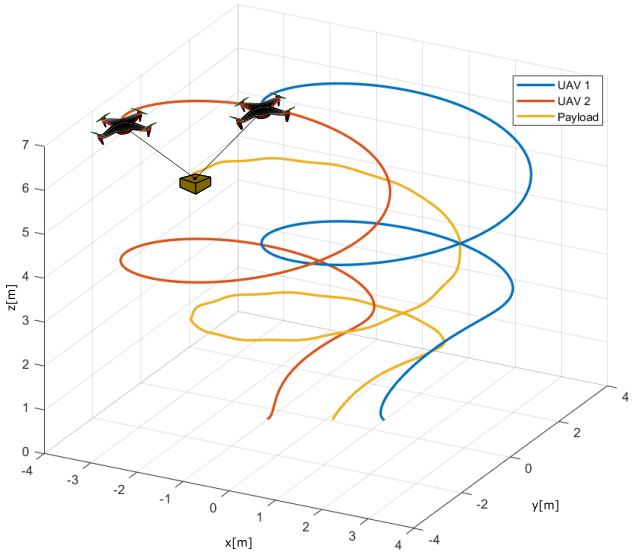


**FIGURE 3.** Cooperative transport of a payload with two UAVs for Case 1.

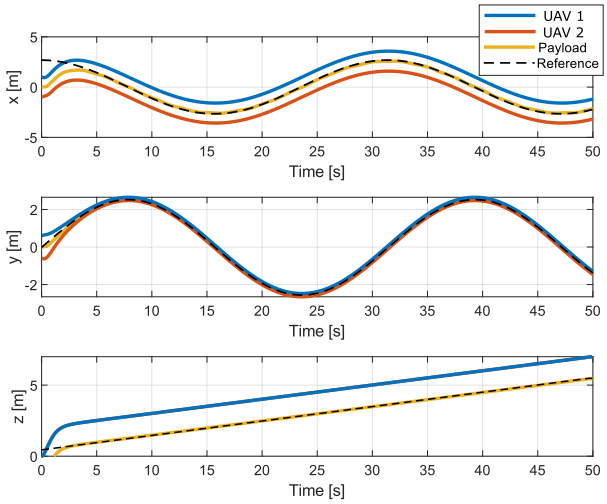


**FIGURE 4.** Temporal response of position of the cooperative transport system.

pattern in a short time and follow the desired trajectory of the virtual leader; moreover, it is observed that the desired formation pattern is successfully maintained while transporting the payload. The time response of the orientation of the two quadcopters is presented in Fig. 5, where it is shown that the Euler angles converge to zero in a short time; it is worth mentioning that the Euler angles are maintained at zero because it is the value that was assigned to the desired orientation of the quadcopters.

The formation errors of both quadcopters are displayed in Fig. 6, from which it can be seen that errors $e_i^x$ and $e_i^y$ converge to the origin at time $t = 5\,\text{s}$, while error $e_i^z$ converges to the origin in a shorter time $t = 3\,\text{s}$. This is explained by the underactuated property of the quadcopters since errors $e_i^x$ and $e_i^y$ belong to the underactuated control subsystem, which has only two control actions for four outputs. In comparison, error $e_i^z$ belongs to the fully actuated control subsystem, which has

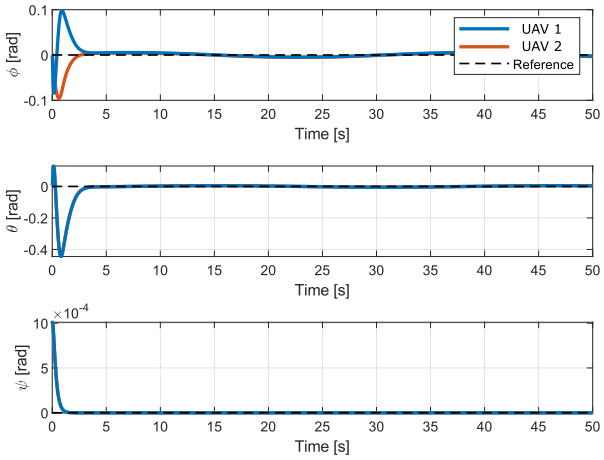


**FIGURE 5.** Temporal response of quadcopters orientation.

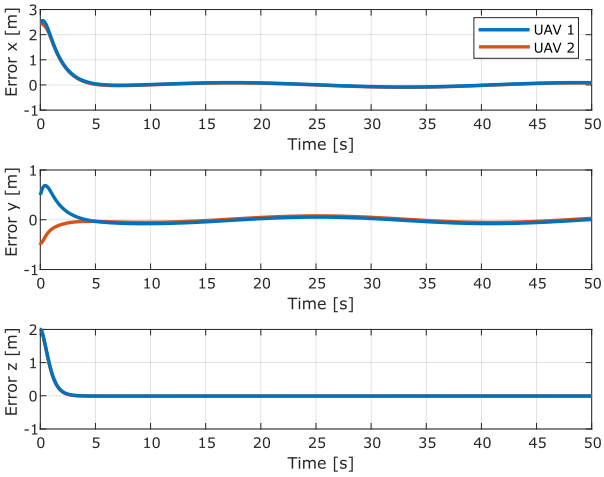


**FIGURE 6.** Temporal response to formation errors.

two control actions for two outputs. Despite this, the control strategy proposed in this paper achieves that the formation errors converge to the origin in a short time and stabilize at the origin, even with the rope tension forces generated by the payload weight.

The estimation of the tension forces of the two ropes acting on each quadcopter is presented in Fig. 7, where the high initial values are due to the initial movements of the two quadcopters, before they achieve the desired formation pattern. The four control inputs $(U_1, U_2, U_3, U_4)$ designed in (22) and (39), are presented in Fig. 8. It can be seen that the total thrust $U_1$ is finally around 22.091 N, which is equal to the gravity force of the quadcopter attached to the payload. The rest control inputs $(U_2, U_3, U_4)$ are maintained at (0, 0, 0) N.m respectively.

### B. CASE 2: WITH DISTURBANCES

In this case, lumped disturbances are considered as; **(i)** Rope tension forces $\mathbb{T} = [\mathbb{T}_x, \mathbb{T}_y, \mathbb{T}_z]^T$. **(ii)** External wind gusts that are injected into the translational and rotational dynamics of the underactuated quadcopters, and are

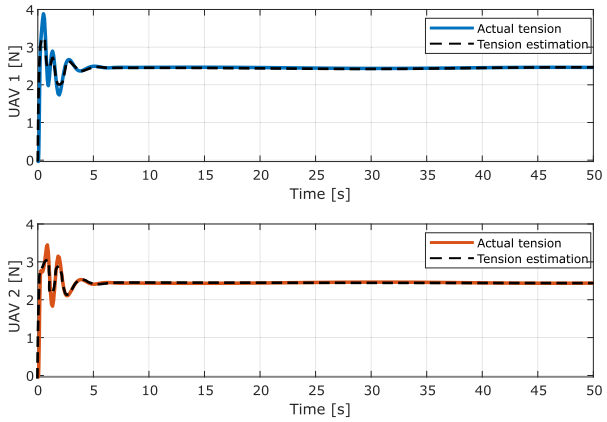


**FIGURE 7.** Estimation of rope tensions.

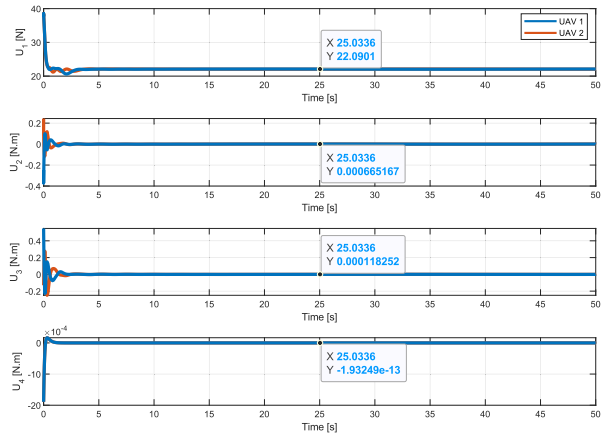


**FIGURE 8.** Control inputs for each quadcopter.

defined respectively as $\delta_p = [0.5 + 0.15\sin(0.5\pi t), 0.5 + 0.15\sin(0.5\pi t), 0.2\sin(0.5\pi t)]^T$N, $\delta_\Theta = [0.1\cos(0.01\ t), 0.1\cos(0.05\pi t), 0.1\cos(0.2\pi t)]^T$ N.m. **(iii)** Parametric uncertainties of $+30\%$ in the mass $m_{qi}$ and moments of inertia $J_i = diag(J_x, J_y, J_z)$. The reference trajectory for the virtual leader is chosen as $\xi_L^d = [2.5\cos(0.2t), 2.5\sin(0.4t), 3.267]^T$m. Assuming that the desired orientation for each quadcopter is the same as in Case 1.

The simulation results are presented in Figs. 9-14. In Fig. 9 illustrates a three-dimensional view of the cooperative transport of a payload following an $\infty$-shaped trajectory in the presence of lumped disturbances; clearly, it can be seen that safe transport of the payload without oscillations is achieved.

The Fig. 10 displays the temporal response of the position of the cooperative transport system; as in the previous case, it can be seen that the quadcopters and the payload achieve the desired formation pattern and maintain stability following the desired trajectory of the virtual leader. Fig. 11 displays the temporal response of the orientation of the two quadcopters; in the same way, the Euler angles converge to their desired values in a short time. However, orientation $\phi_1, \phi_2$ does not converge completely to zero but remains in a reasonable range.

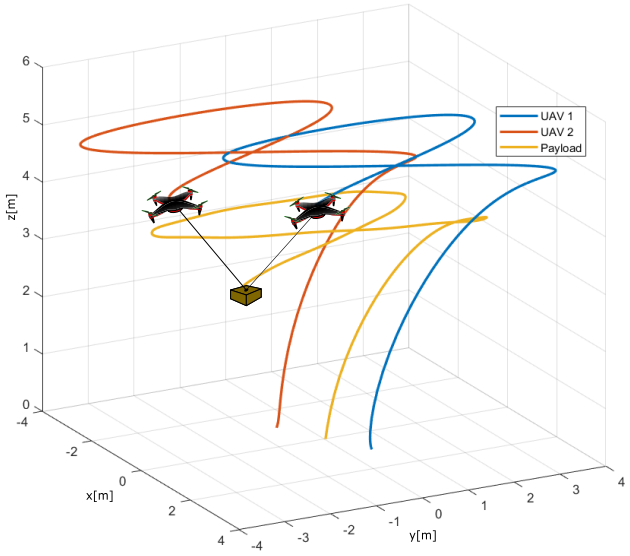


**FIGURE 9.** Cooperative transport of a payload with two UAVs for Case 2.

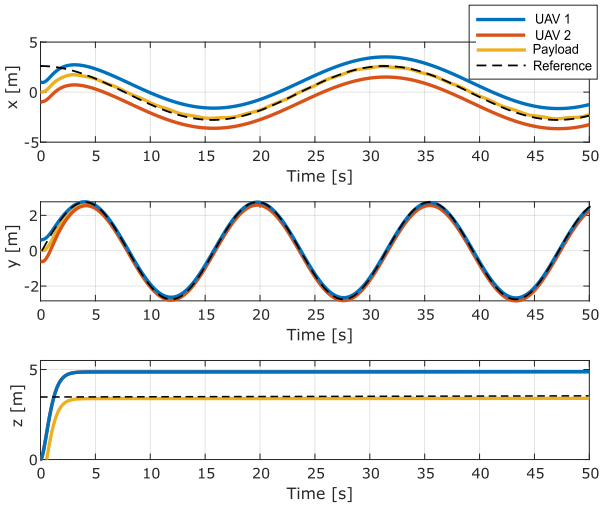


**FIGURE 10.** Temporal response of position of the cooperative transport system with disturbances.

From the above Figs. 10-11, it can be observed that the lumped disturbances injected into the quadcopter dynamics do not affect the stability of the cooperative transport system of a payload. To support this statement, the formation errors of both quadcopters are presented in Fig. 12, where it can be observed that the formation errors are still maintained close to the origin, with small overshoots in errors $e_i^x$ and $e_i^y$; the fact of the presence of lumped disturbances in the three axes explains this. Moreover, the convergence time of errors $e_i^x$ and $e_i^y$ is longer than error $e_i^z$; as mentioned in the previous case, this is due to the underactuated property of the quadcopters. Despite this, the stability and the desired formation pattern of the cooperative transport system are still guaranteed, demonstrating the robustness of the control strategy proposed in this paper against lumped disturbances.

The estimation of the disturbances lumped along the three axes are presented in Fig. 13. The four control inputs

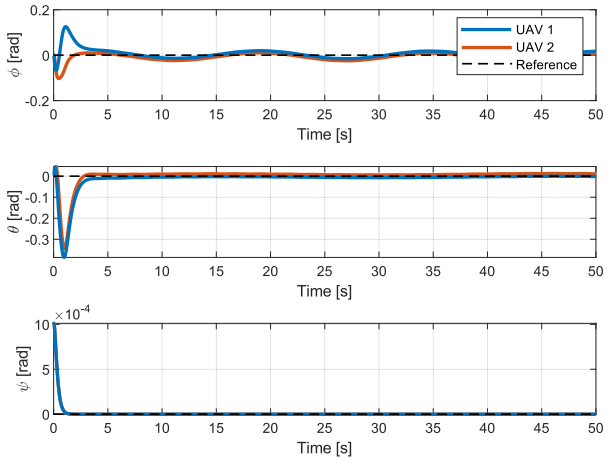


**FIGURE 11.** Temporal response of quadcopters orientation with disturbances.

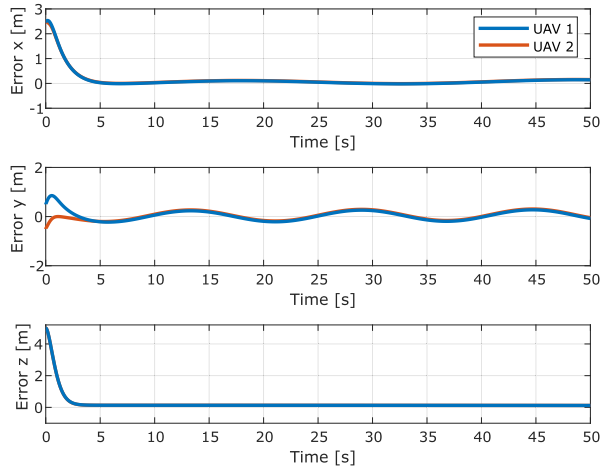


**FIGURE 12.** Temporal response to formation errors.

$(U_1, U_2, U_3, U_4)$ designed in (22) and (39) are presented in Fig. 14. In this case the total thrust is $U_1 = 25.054$ N, as can be seen the magnitude is higher than in Case 1 ($U_1 = 22.091$ N), this is explained by the fact that in this case a parametric uncertainty of $+30\%$ on the mass $m_{qi}$ and moments of inertia $J_i = diag(J_x, J_y, J_z)$ was considered, which leads the controller to make a greater effort to achieve the stability of the cooperative transport system. The rest control inputs $(U_2, U_3, U_4)$ are maintained at $(0, 0, 0)$ N.m respectively.

## VI. CONCLUSION

This paper presented a novel control design for the cooperative transport of a payload suspended by ropes using two quadcopters which are considered underactuated mechanical systems subject to lumped disturbances. The control structure was divided into two subsystems: fully actuated and underactuated. An integral sliding mode adaptive control strategy was proposed for the fully actuated subsystem, and an adaptive control strategy based on the combination of Backstepping and sliding mode was proposed for the underactuated control subsystem. The control parameters of the sliding surfaces

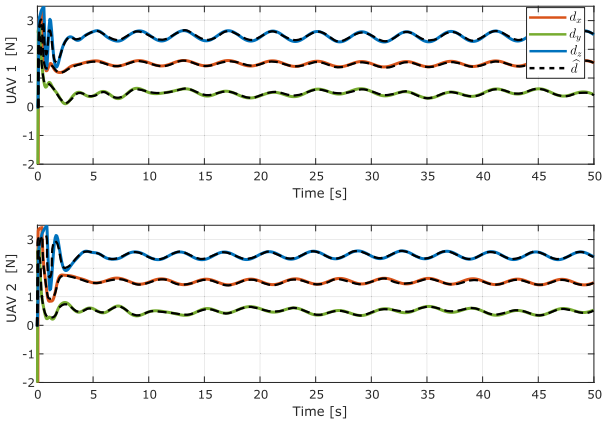


**FIGURE 13.** Estimation of external disturbances.

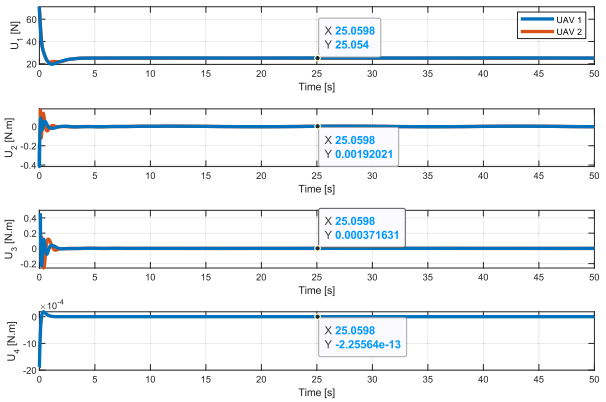


**FIGURE 14.** Control inputs for each quadcopter.

were adaptively tuned with a neural network by the backpropagation algorithm. In addition, a nonlinear disturbance observer was incorporated to estimate and compensate for lumped disturbances (string tension forces, wind gusts, parametric uncertainties). Simulation results demonstrate that the controller proposed in this paper successfully transported the payload safely and without oscillations using two underactuated quadcopters. Moreover, the desired formation pattern was successfully maintained throughout the flight task, thus guaranteeing the stability of the cooperative transport system, even in the presence of disturbances such as rope tensions, wind gusts, and parametric uncertainties.

## APPENDIX A
## PARAMETER VALUES USED FOR THE SIMULATIONS

**TABLE 1.** Physical parameters of the cooperative system.

| Parameter | Value | Unit |
|---|---|---|
| $m_{qi}$ | 2 | $Kg$ |
| $J_{ri}$ | 0.015 | $Kg.m^2$ |
| $J_x$ | 0.018125 | $Kg.m^2$ |
| $J_y$ | 0.018125 | $Kg.m^2$ |
| $J_z$ | 0.035 | $Kg.m^2$ |
| $\varsigma$ | 0.15 | $m$ |
| $m_p$ | 0.5 | $Kg$ |
| $l_1 = l_2$ | 2 | $m$ |
| $\kappa$ | 1 | – |

**TABLE 2.** Control parameters.

| Parameter | Value | Parameter | Value | Parameter | Value |
|---|---|---|---|---|---|
| $\Xi_{1,0}$ | 4 | $\Xi_{9,0}$ | 0.1 | $\omega_{\theta,0}$ | 1 |
| $\Xi_{2,0}$ | 0.1 | $\Xi_{10,0}$ | 50 | $\omega_{z,0}$ | 0.01 |
| $\Xi_{3,0}$ | 4 | $\Xi_{11,0}$ | 30 | $\eta_{z,\psi}$ | 2 |
| $\Xi_{4,0}$ | 0.1 | $\Xi_{12,0}$ | 2 | $\eta_{\phi,\theta}$ | 5 |
| $\Xi_{5,0}$ | 40 | $\Xi_{13,0}$ | 10 | $k_{s_\phi}$ | 0.75 |
| $\Xi_{6,0}$ | 25 | $\Xi_{14,0}$ | 0.1 | $k_{s_\theta}$ | 2 |
| $\Xi_{7,0}$ | 2 | $\varepsilon_0$ | 5 | $\alpha_{\phi,\theta}$ | 1.5 |
| $\Xi_{8,0}$ | 15 | $\omega_{\phi,0}$ | 6 | $\lambda$ | 15 |

## APPENDIX B
## ALGORITHMS

**Algorithm 1** Algorithm for Cooperative Transport System

**Require:**

Define quadcopters and payload parameters:
$m_{qi}, m_p, J_x, J_y, J_z, J_{ri}, \varsigma, \kappa$
Define the parameters of the Udwadia-Kalaba equation:
$l_i, \alpha, \beta$
Define controller parameters:
$\Xi_{\sigma,0}, \varepsilon_{\phi,0}, \varepsilon_{\theta,0}, \varepsilon_{\psi,0}, \varepsilon_{z,0}, \omega_{\phi,0}, \omega_{\theta,0}, \omega_{\psi,0}, \omega_{z,0}, \eta_{\phi,\theta}, \eta_{z,\psi}, k_{s_\phi}, k_{s_\theta}, \alpha_{\phi,\theta}$
Define formation distance: $\Delta_x, \Delta_y, \Delta_z$
**while** Repeat **do**
    **Fully actuated control subsystem**
    Acquires current status: $z_i, \psi_i$
    Error computation: $e_i^z, e_i^\psi$
    Derivation of errors: $\dot{e}_i^z, \dot{e}_i^\psi$
    Define sliding surfaces: $s_{z_i}, s_{\psi_i}$
    Derivation of sliding surfaces: $s_{z_i}, s_{\psi_i}$
    Calculation of control inputs: $U_{1i}, U_{4i}$
    **Neural network**
    Calculate adaptive parameters of $s_{z_i}$: $\varepsilon_z$, $\Xi_1$, $\Xi_2$
    Calculate adaptive parameters of $s_{\psi_i}$: $\varepsilon_\psi$, $\Xi_3$, $\Xi_4$
    **Underactuated control subsystem**
    Acquires current status: $x_i, y_i, \phi_i, \theta_i$
    Error computation: $e_{1i}^x, e_{1i}^y, e_{1i}^\phi, e_{1i}^\theta$
    Derivation of errors: $\dot{e}_{1i}^x, \dot{e}_{1i}^y, \dot{e}_{1i}^\phi, \dot{e}_{1i}^\theta$
    Define sliding surfaces: $s_{\phi_i}, s_{\theta_i}$
    Derivation of sliding surfaces: $\dot{s}_{\phi_i}, \dot{s}_{\theta_i}$
    Calculation of control inputs: $U_{2i}, U_{3i}$
    **Neural network**
    Calculate adaptive parameters of $s_{\phi_i}$:
    $\varepsilon_\phi$, $\Xi_5$, $\Xi_6$, $\Xi_7$, $\Xi_8$, $\Xi_9$
    Calculate adaptive parameters of $s_{\theta_i}$:
    $\varepsilon_\theta$, $\Xi_{10}$, $\Xi_{11}$, $\Xi_{12}$, $\Xi_{13}$, $\Xi_{14}$
    **Nonlinear disturbance observer**
    Acquire control inputs: $U_{1i}, U_{2i}, U_{3i}, U_{4i}$
    Acquire current status: $x_i, y_i, z_i, \phi_i, \theta_i, \psi_i$
    Observer output: $\hat{d}_x, \hat{d}_y, \hat{d}_z$
**end while**

## ACKNOWLEDGMENT

The authors would like to thank the Instituto de Investigación Astronómico y Aeroespacial Pedro Paulet (IAAPP) - UNSA for permitting this research to be carried out.

## REFERENCES

[1] V. Kumar and N. Michael, "Opportunities and challenges with autonomous micro aerial vehicles," *Int. J. Robot. Res.*, vol. 31, no. 11, pp. 1279–1291, Sep. 2012.
[2] D. K. D. Villa, A. S. Brandão, and M. Sarcinelli-Filho, "A survey on load transportation using multirotor UAVs," *J. Intell. Robotic Syst.*, vol. 98, no. 2, pp. 267–296, May 2020.
[3] J. Braun, S. D. Gertz, A. Furer, T. Bader, H. Frenkel, J. Chen, E. Glassberg, and D. Nachman, "The promising future of drones in prehospital medical care and its application to battlefield medicine," *J. Trauma Acute Care Surgery*, vol. 87, no. 1, pp. 28–34, Jul. 2019.
[4] M. Mammarella, L. Comba, A. Biglia, F. Dabbene, and P. Gay, "Cooperation of unmanned systems for agricultural applications: A theoretical framework," *Biosyst. Eng.*, vol. 223, pp. 61–80, Nov. 2022.
[5] A. Konert, J. Smereka, and L. Szarpak, "The use of drones in emergency medicine: Practical and legal aspects," *Emergency Med. Int.*, vol. 2019, pp. 1–5, Dec. 2019.
[6] B. J. Emran and H. Najjaran, "A review of quadrotor: An underactuated mechanical system," *Annu. Rev. Control*, vol. 46, pp. 165–180, Jan. 2018.
[7] R. Olfati-Saber, "Nonlinear control of underactuated mechanical systems with application to robotics and aerospace vehicles," Doctoral dissertation, Massachusetts Inst. Technol., Cambridge, MA, USA, 2001.
[8] K. Klausen, T. I. Fossen, and T. A. Johansen, "Nonlinear control with swing damping of a multirotor UAV with suspended load," *J. Intell. Robotic Syst.*, vol. 88, nos. 2–4, pp. 379–394, Dec. 2017.
[9] X. Liang, Y. Fang, N. Sun, and H. Lin, "Dynamics analysis and time-optimal motion planning for unmanned quadrotor transportation systems," *Mechatronics*, vol. 50, pp. 16–29, Apr. 2018.
[10] G. Yu, D. Cabecinhas, R. Cunha, and C. Silvestre, "Nonlinear backstepping control of a quadrotor-slung load system," *IEEE/ASME Trans. Mechatronics*, vol. 24, no. 5, pp. 2304–2315, Oct. 2019.
[11] M. Doakhan, M. Kabganian, and A. Azimi, "Cooperative payload transportation with real-time formation control of multi-quadrotors in the presence of uncertainty," *J. Franklin Inst.*, vol. 360, no. 2, pp. 1284–1307, Jan. 2023.
[12] H. M. H. Abdoli, M. Najafi, I. Izadi, and F. Sheikholeslam, "Sliding mode approach for formation control of multi-agent systems with unknown nonlinear interactions," *ISA Trans.*, vol. 80, pp. 65–72, Sep. 2018.
[13] O. Mechali, L. Xu, X. Xie, and J. Iqbal, "Theory and practice for autonomous formation flight of quadrotors via distributed robust sliding mode control protocol with fixed-time stability guarantee," *Control Eng. Pract.*, vol. 123, Jun. 2022, Art. no. 105150.
[14] O. Mechali, L. Xu, and X. Xie, "Nonlinear homogeneous sliding mode approach for fixed-time robust formation tracking control of networked quadrotors," *Aerosp. Sci. Technol.*, vol. 126, Jul. 2022, Art. no. 107639.
[15] G. Muscio, F. Pierri, M. A. Trujillo, E. Cataldi, G. Antonelli, F. Caccavale, A. Viguria, S. Chiaverini, and A. Ollero, "Coordinated control of aerial robotic manipulators: Theory and experiments," *IEEE Trans. Control Syst. Technol.*, vol. 26, no. 4, pp. 1406–1413, Jul. 2018.
[16] H. Lee, H. Kim, and H. J. Kim, "Planning and control for collision-free cooperative aerial transportation," *IEEE Trans. Autom. Sci. Eng.*, vol. 15, no. 1, pp. 189–201, Jan. 2018.
[17] H. Lee and H. J. Kim, "Constraint-based cooperative control of multiple aerial manipulators for handling an unknown payload," *IEEE Trans. Ind. Informat.*, vol. 13, no. 6, pp. 2780–2790, Dec. 2017.
[18] Y. Liu, F. Zhang, P. Huang, and X. Zhang, "Analysis, planning and control for cooperative transportation of tethered multi-rotor UAVs," *Aerosp. Sci. Technol.*, vol. 113, Jun. 2021, Art. no. 106673.
[19] H. Sayyaadi and A. Soltani, "Modeling and control for cooperative transport of a slung fluid container using quadrotors," *Chin. J. Aeronaut.*, vol. 31, no. 2, pp. 262–272, Feb. 2018.
[20] K. Sreenath and V. Kumar, "Dynamics, control and planning for cooperative manipulation of payloads suspended by cables from multiple quadrotor robots," *Rn*, vol. 1, p. r3, Jun. 2013.
[21] F. Arab, F. A. Shirazi, and M. R. H. Yazdi, "Planning and distributed control for cooperative transportation of a non-uniform slung-load by multiple quadrotors," *Aerosp. Sci. Technol.*, vol. 117, Oct. 2021, Art. no. 106917.
[22] D. K. D. Villa, A. S. Brandao, R. Carelli, and M. Sarcinelli-Filho, "Cooperative load transportation with two quadrotors using adaptive control," *IEEE Access*, vol. 9, pp. 129148–129160, 2021.
[23] J. Gimenez, D. C. Gandolfo, L. R. Salinas, C. Rosales, and R. Carelli, "Multi-objective control for cooperative payload transport with rotorcraft UAVs," *ISA Trans.*, vol. 80, pp. 491–502, Sep. 2018.

[24] X. Li, J. Zhang, and J. Han, "Trajectory planning of load transportation with multi-quadrotors based on reinforcement learning algorithm," *Aerosp. Sci. Technol.*, vol. 116, Sep. 2021, Art. no. 106887.
[25] K. K. Dhiman, M. Kothari, and A. Abhishek, "Autonomous load control and transportation using multiple quadrotors," *J. Aerosp. Inf. Syst.*, vol. 17, no. 8, pp. 417–435, Aug. 2020.
[26] B. Shirani, M. Najafi, and I. Izadi, "Cooperative load transportation using multiple UAVs," *Aerosp. Sci. Technol.*, vol. 84, pp. 158–169, Jan. 2019.
[27] S. O. Ariyibi and O. Tekinalp, "Quaternion-based nonlinear attitude control of quadrotor formations carrying a slung load," *Aerosp. Sci. Technol.*, vol. 105, Oct. 2020, Art. no. 105995.
[28] Y. Alothman, M. Guo, and D. Gu, "Using iterative LQR to control two quadrotors transporting a cable-suspended load," *IFAC-PapersOnLine*, vol. 50, no. 1, pp. 4324–4329, Jul. 2017.
[29] I. H. B. Pizetta, A. S. Brandão, and M. Sarcinelli-Filho, "Avoiding obstacles in cooperative load transportation," *ISA Trans.*, vol. 91, pp. 253–261, Aug. 2019.
[30] I. H. B. Pizetta, A. S. Brandao, and M. Sarcinelli-Filho, "Cooperative quadrotors carrying a suspended load," in *Proc. Int. Conf. Unmanned Aircr. Syst. (ICUAS)*, Jun. 2016, pp. 1049–1055.
[31] I. H. B. Pizetta, A. S. Brandao, and M. Sarcinelli-Filho, "Cooperative load transportation using three quadrotors," in *Proc. Int. Conf. Unmanned Aircr. Syst. (ICUAS)*, Jun. 2019, pp. 644–650.
[32] G. Tartaglione, E. D'Amato, M. Ariola, P. S. Rossi, and T. A. Johansen, "Model predictive control for a multi-body slung-load system," *Robot. Auto. Syst.*, vol. 92, pp. 1–11, Jun. 2017.
[33] X. Liang, Z. Su, W. Zhou, G. Meng, and L. Zhu, "Fault-tolerant control for the multi-quadrotors cooperative transportation under suspension failures," *Aerosp. Sci. Technol.*, vol. 119, Dec. 2021, Art. no. 107139.
[34] E.-H. Zheng, J.-J. Xiong, and J.-L. Luo, "Second order sliding mode control for a quadrotor UAV," *ISA Trans.*, vol. 53, no. 4, pp. 1350–1356, Jul. 2014.
[35] J.-J. Xiong and E.-H. Zheng, "Position and attitude tracking control for a quadrotor UAV," *ISA Trans.*, vol. 53, no. 3, pp. 725–731, May 2014.
[36] J.-J. Xiong and G.-B. Zhang, "Global fast dynamic terminal sliding mode control for a quadrotor UAV," *ISA Trans.*, vol. 66, pp. 233–240, Jan. 2017.
[37] H. Razmi and S. Afshinfar, "Neural network-based adaptive sliding mode control design for position and attitude control of a quadrotor UAV," *Aerosp. Sci. Technol.*, vol. 91, pp. 12–27, Aug. 2019.
[38] S. Ullah, Q. Khan, A. Mehmood, S. A. M. Kirmani, and O. Mechali, "Neuro-adaptive fast integral terminal sliding mode control design with variable gain robust exact differentiator for under-actuated quadcopter UAV," *ISA Trans.*, vol. 120, pp. 293–304, Jan. 2022.
[39] T. Madani and A. Benallegue, "Backstepping control for a quadrotor helicopter," in *Proc. IEEE/RSJ Int. Conf. Intell. Robots Syst.*, Oct. 2006, pp. 3255–3260.
[40] M. Huang, B. Xian, C. Diao, K. Yang, and Y. Feng, "Adaptive tracking control of underactuated quadrotor unmanned aerial vehicles via backstepping," in *Proc. Amer. Control Conf.*, Jun. 2010, pp. 2076–2081.
[41] Ö. Bingöl and H. M. Guzey, "Neuro sliding mode control of quadrotor UAVs carrying suspended payload," *Adv. Robot.*, vol. 35, nos. 3–4, pp. 255–266, Feb. 2021.
[42] Ö. Bingöl and H. M. Guzey, "Finite-time neuro-sliding-mode controller design for quadrotor UAVs carrying suspended payload," *Drones*, vol. 6, no. 10, p. 311, Oct. 2022.
[43] O. Mechali, L. Xu, Y. Huang, M. Shi, and X. Xie, "Observer-based fixed-time continuous nonsingular terminal sliding mode control of quadrotor aircraft under uncertainties and disturbances for robust trajectory tracking: Theory and experiment," *Control Eng. Pract.*, vol. 111, Jun. 2021, Art. no. 104806.
[44] K. Klausen, C. Meissen, T. I. Fossen, M. Arcak, and T. A. Johansen, "Cooperative control for multirotors transporting an unknown suspended load under environmental disturbances," *IEEE Trans. Control Syst. Technol.*, vol. 28, no. 2, pp. 653–660, Mar. 2020.
[45] M. Bisgaard, "Modeling, estimation, and control of helicopter slung load system," Dept. Control Eng., Aalborg Univ., Aalborg, Denmark, 2008. [Online]. Available: https://vbn.aau.dk/en/publications/modeling-estimation-and-control-of-helicopter-slung-load-system
[46] W. Ren and R. Beard, *Distributed Consensus in Multi-Vehicle Cooperative Control*. Berlin, Germany: Springer, 2008.
[47] J. Yang, S. Li, and X. Yu, "Sliding-mode control for systems with mismatched uncertainties via a disturbance observer," *IEEE Trans. Ind. Electron.*, vol. 60, no. 1, pp. 160–169, Jan. 2013.
[48] T. D. C. Thanh and K. K. Ahn, "Nonlinear PID control to improve the control performance of 2 axes pneumatic artificial muscle manipulator using neural network," *Mechatronics*, vol. 16, no. 9, pp. 577–587, Nov. 2006.
[49] S. B. F. Asl and S. S. Moosapour, "Adaptive backstepping fast terminal sliding mode controller design for ducted fan engine of thrust-vectored aircraft," *Aerosp. Sci. Technol.*, vol. 71, pp. 521–529, Dec. 2017.
[50] B. Gao, Y.-J. Liu, and L. Liu, "Adaptive neural fault-tolerant control of a quadrotor UAV via fast terminal sliding mode," *Aerosp. Sci. Technol.*, vol. 129, Oct. 2022, Art. no. 107818.

**LUIS F. CANAZA CCARI** received the B.Sc. degree in electronic engineering from Universidad Nacional de San Agustín de Arequipa, Peru, in 2022. He is currently a Junior Researcher of a research project with the National Council of Science, Technology and Technological Innovation (CONCYTEC). His research interests include advanced control systems, UAVs, robotics, and multimodal interfaces.

**PABLO RAUL YANYACHI** (Senior Member, IEEE) received the M.Sc. degree in automatic control from the Polytechnic Institute of Leningrad and the Ph.D. degree in electrical engineering from the Polytechnic School, University of São Paulo, Brazil. He is currently a main Professor with the Department of Electronic Engineering, Universidad Nacional de San Agustín de Arequipa (UNSA). He is the Station Manager of the Nasa Laser Tracking Station TLRS-3, Arequipa, Peru. He is also the Director of Instituto de Investigación Astronómico y Aeroespacial Pedro Paulet (IAAPP), UNSA.